Biochimica et Biophysica Acta 1830 (2013) 2960–2969

Contents lists available at SciVerse ScienceDirect

Biochimica et Biophysica Acta

journal homepage: www.elsevier.com/locate/bbagen

In silico and *in vitro* characterization of anti-amyloidogenic activity of vitamin K3 analogues for Alzheimer's disease

Pham Dinh Quoc Huy [a,1], Yao-Chung Yu [b,1], Son Tung Ngo [a,c,1], Tran Van Thao [d], Chin-piao Chen [e], Mai Suan Li [c,*], Yi-Cheng Chen [b,f,**]

[a] Institute for Computational Science and Technology, 6 Quarter, Linh Trung Ward, Thu DucDistrict, Ho Chi Minh City, Viet Nam
[b] Institute of Medical Biotechnology, Tzu Chi University, Hualien, 970, Taiwan
[c] Institute of Physics, Polish Academy of Sciences, Al. Lotnikow 32/46, 02-668 Warsaw, Poland
[d] Department of Physics, University of Sciences at Ho Chi Minh City, 227 Nguyen Van Cu, Dist. 5, Viet Nam
[e] Department of Chemistry, National Dong Hwa University, Hualien 957, Taiwan
[f] Department of Medicine, Mackay Medical College, New Taipei City, 225, Taiwan

ARTICLE INFO

Article history:
Received 27 July 2012
Received in revised form 19 December 2012
Accepted 21 December 2012
Available online 5 January 2013

Keywords:
Amyloid-beta
Degenerative disease
Alzheimer disease
Vitamin K3 analog
Anti-amyloidogenic activity
Molecular dynamics simulation

ABSTRACT

Background: Aggregation of amyloid-beta (Aβ) has been proposed as the main cause of Alzheimer's disease (AD). Vitamin K deficiency has been linked to the pathogenesis of AD. Therefore, 15 synthesized vitamin K3 (VK3) analogues were studied for their anti-amyloidogenic activity.
Methods: Biological and spectroscopic assays were used to characterize the effect of VK3 analogues on amyloidogenic properties of Aβ, such as aggregation, free radical formation, and cell viability. Molecular dynamics simulation was used to calculate the binding affinity and mode of VK3 analogue binding to Aβ.
Results: Both numerical and experimental results showed that several VK3 analogues, including VK3-6, VK3-8, VK3-9, VK3-10, and VK3-224 could effectively inhibit Aβ aggregation and conformational conversion. The calculated inhibition constants were in the μM range for VK3-10, VK3-6, and VK3-9 which was similar to the IC_{50} of curcumin. Cell viability assays indicated that VK3-9 could effectively reduce free radicals and had a protective effect on cytotoxicity induced by Aβ.
Conclusions: The results clearly demonstrated that VK3 analogues could effectively inhibit Aβ aggregation and protect cells against Aβ induced toxicity. Modified VK3 analogues can possibly be developed as effective anti-amyloidogenic drugs for the treatment of AD.
General significance: VK3 analogues effectively inhibit Aβ aggregation and are highly potent as anti-amyloidogenic drugs for therapeutic treatment of AD.

1. Introduction

Alzheimer's disease (AD) is the most common form of dementia within the senior population, and is characterized pathologically by the progressive intracerebral accumulation of amyloid-beta (Aβ) peptides [1,2]. These peptides are proteolytic byproducts of the Aβ protein precursor, and are most commonly composed of 40 (Aβ1−40) and 42 (Aβ1−42) amino acids. Aβ peptides appear to be unstructured in their monomeric state but aggregate to form fibrils with an ordered cross β-sheet pattern [3–6]. Increasing evidence from recent studies indicates that soluble oligomers as well as mature fibrils are the toxic agents [7–9].

Presently there is no cure or treatment for AD, and significant effort has been made to find drugs to cope with this disease. Based on the amyloid cascade hypothesis, small molecules which enable to stabilize the conformation of monomeric Aβ or to inhibit and reverse misfolding and aggregation could be potent drug candidates for the therapeutic treatment of AD [4,5,7,10–13]. In general, two classes of inhibitors are known, bioactive molecules and drugs unrelated to AD [10]. Many of the known compounds such as curcumin [14], polyphenols from wine [15], apomorphine [16], omega-3 fatty acids [17], vitamin A, and β-carotene [18] belong to the first class. The drugs included in the second class are anti-inflammatory [19] and anti-Parkinson agents such as dopamine, selegiline, and L-dopa [20,21].

Moreover, based on their anti-amyloidogenic activities, the compounds which inhibit Aβ aggregation can be further divided into four groups. The strongest anti-amyloidogenic group, including dopamine

Abbreviations: Aβ, amyloid-beta; VK, vitamin K; AD, Alzheimer's disease; IC_{50}, half maximal inhibitory concentration; ApoE, apolipoprotein E; MD, molecular dynamics; MM-PBSA, molecular mechanics-Poisson−Boltzmann surface area; SI, supplemental information; DCFH-DA, dichlorofluorescein diacetate; DCF, dichlorofluorescein; ThT, thioflavin-T; FT-IR, Fourier-transform infrared; ROS, reactive oxygen species

* Corresponding author. Tel.: +48 22 8436601x3326; fax: +48 22 8475223.
** Correspondence to: Y.-C. Chen, Department of Medicine, Mackay Medical College, New Taipei City, 225, Taiwan. Tel.: +886 2 26360303; fax: +886 2 26361295.
E-mail addresses: masli@ifpan.edu.pl (M.S. Li), chen15@mail.mmc.edu.tw (Y.-C. Chen).

[1] Dinh Quoc Huy, Yao-Chung Yu, and Son Tung Ngo contributed equally to the work.

0304-4165/$ – see front matter © 2013 Elsevier B.V. All rights reserved.
http://dx.doi.org/10.1016/j.bbagen.2012.12.026

and tannic acid, has a half maximal inhibitory concentration (IC_{50}) value of 0.01 μM [15,20,22]. The second group, including nordihydroguaiaretic acid, curcumin, and myricetin, has an IC_{50} value of 0.1 μM [14,20,23]. The third group, including L-dopa and β-carotene, has an IC_{50} value of 1 μM [18,20]. The fourth group, including tetracycline and rifampicin, has an IC_{50} value of 10 μM [24,25]. The effects of the antioxidant vitamins A, B2, B6, C, and E on the inhibition of Aβ aggregation has been studied [18]. Among these vitamins, vitamin A shows the most potent inhibition of Aβ aggregation *in vitro*. The IC_{50} of vitamin A is approximately 0.1 μM [18], whereas the IC_{50} for vitamins C and E are much higher, at around 200–500 μM for vitamin C [26] and 10 μM for vitamin E [21].

The possible role of vitamin K in the pathogenesis of AD was first reported by Allison [27]. When compared to other apolipoprotein E (ApoE 2 and ApoE3) genotypes, the concentration of vitamin K was lower in the circulating blood of ApoE4 carriers, which is a genetic risk factor for late-onset AD. Therefore, it was suggested that vitamin K deficiency may contribute to the pathogenesis of AD and that vitamin K supplementation may have a beneficial effect in preventing or treating AD. Although vitamin K has been shown to regulate functions in the brain, such as sulfotransferase activity, and the activity of a growth factor/tyrosine kinase receptor, the molecular mechanism of action of vitamin K on AD remains unclear. This could be due to a lack of interest because of its neurotoxicity.

In the present study, we experimentally studied the effects of 15 vitamin K3 (VK3) analogues on Aβ1–40 aggregation and cellular toxicity. Although many VK3 analogues such as VK3–9, VK3–10, and VK3–6 inhibited the aggregation of Aβ1–40, only VK3–9 was able to protect cells against Aβ1–40 induced toxicity. The effective dose of VK3–9 was approximately 0.1 μM, which is as effective as amyloidogenic compounds such as curcumin [14,15,21]. Further simulation analyses revealed that the electrostatic and van der Waals forces, rather than hydrogen bonding networks, are the key factors governing binding affinities of VK3 analogues to Aβ1–40. The binding energies of Aβ1–40–VK3 analogue complexes displayed a high correlation with the experimental aggregation rates. In conclusion, although most VK3 analogues did not protect cells against Aβ induced toxicity, both simulation and experimental results suggest that VK3–9 is a potent compound for preventing aggregation of amyloid peptides. Other VK3 analogues such as VK3–10 and VK3–6 could be further modified for potential use as therapeutic drugs to treat AD.

2. Material and methods

2.1. Docking of Vitamin K3 analogues to Aβ1–40

Because Aβ peptides are highly aggregation prone in water, their monomeric structures have not yet been experimentally resolved. Therefore, to obtain suitable Aβ1–40 structures in an aqueous environment for use in simulation of binding of VK3 analogues, we modeled the Aβ structure in water using the PDB code 1BA4 [28] as the initial structural model. This model is Aβ1–40 determined in the water-micelle environment. The structure taken from 1BA4 was first heated to $T=$ 500 K. The 5 ns MD simulations [see Supplemental Information (SI) for details on MD simulations] were carried out at this temperature until random coil structures were obtained in explicit water using the GROMOS96 43a1 force field [29]. A random coil structure was used as the starting configuration for subsequent 300 ns MD simulations at $T=310$ K. Snapshots collected at equilibrium during the last 200 ns were grouped by the Cα-RMSD conformational clustering method implemented in the Gromacs software. With the clustering tolerance of 1 Å, 5 representative structures with the lowest energy (Fig. S3 in SI) were used for further docking of VK3 analogues to Aβ1–40.

To dock VK3 analogues to full-length Aβ1–40, both Aβ1–40 and VK3 analogues were prepared as PDBQT files using AutodockTools 1.5.4 [30]. The Autodock Vina version 1.1 was employed [31], as it is much more efficient than Autodock 4.0. To describe atomic interactions, a modified version of the CHARMM force field was implemented [32]. In the Autodock Vina software the Broyden–Fletcher–Goldfarb–Shanno method was employed for local optimization [33]. To obtain reliable results, the exhaustiveness of global search was set to 400, and the maximum energy difference between the best and worse binding mode was chosen as 7. Twenty binding modes (20 modes of docking) were generated with random starting positions of each VK3 analogue, which had fully flexible torsional degrees of freedom. The center grids were placed at the center of the mass of Aβ1–40, and grid dimensions were 60×40×40, which are large enough to cover the entire Aβ1–40. In this approach, the binding energy was the average of five obtained Aβ1–40–VK3 analogue complex models (Fig. S5 in SI).

2.2. Molecular mechanics–Poisson–Boltzmann surface area

The details of MM-PBSA are given in SI. Overall, in this method the binding free energy (ΔG_{bind}) of ligand to receptor is given as:

$$\Delta G_{bind} = \Delta E_{elec} + \Delta E_{vdw} + \Delta G_{sur} + \Delta G_{PB} - T\Delta S \quad (1)$$

where ΔE_{elec} and ΔE_{vdw} are contributions from electrostatic and van der Waals interactions, respectively. ΔG_{sur} and ΔG_{PB} are nonpolar and polar solvation energies. The entropic contribution of $T\Delta S$ was estimated using the normal mode approximation (see SI for more details). To calculate ΔG_{bind}, the MD simulations were carried out using the GROMOS force field 43a1 as described in SI. The structures of Aβ1–40–VK3 analogue complexes obtained in the best docking mode (see Fig. 6 and snapshot 5 in Fig. S4) were used as starting configurations for MD simulations. For each system, 4—6 MD trajectories of approximately 100 ns were generated. Snapshots collected in equilibrium were used to compute the binding free energy given by Eq. (1).

2.3. Synthesis of vitamin K3 analogues

The synthesis procedures of vitamin K3 analogues shown in Fig. 1 are described elsewhere [34]. Analogues were kindly provided by Professor C. P. Chen of National Dong Hwa University.

2.4. Synthesis and purification of Aβ1–40

Aβ1–40 was synthesized in a solid-phase peptide synthesizer (ABI 433A) using standard FMOC protocols with HMP resin. After cleavage from the resin with a mixture of trifluoroacetic acid/H_2O/ethanedithiol thiol anisole/phenol, the peptides were extracted with 1:1 (v:v) ether: H_2O containing 0.1% 2-mercaptothanol. The synthesized Aβ1–40 peptides were purified using a C_{18} reverse-phase column with a linear gradient from 0% to 78% acetonitrile. Peptide purity was over 95% as

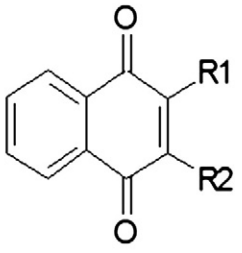

VK3-1 : R1=-SC_2H_4OH, R2=-CH_3
VK3-2 : R1=-SC_3H_6OH, R2=-CH_3
VK3-3 : R1=-SC_4H_8OH, R2=-CH_3
VK3-4 : R1=-$SC_6H_{12}OH$, R2=-CH_3
VK3-5 : R1=-$SC_{11}H_{22}OH$, R2=-CH_3
VK3-6 : R1=-SC_2H_4COOH, R2=-CH_3
VK3-8 : R1=-$SCH_2CHOHCH_3$, R2=-CH_3
VK3-9 : R1=- $SCH_2CHOHCH_2OH$, R2=-CH_3
VK3-10 : R1=-S (C_6H_4)OH, R2=-CH_3
VK3-199 : R1=-SC_2H_4OH, R2=-H
VK3-221 : R1=-OH, R2=-CH_3
VK3-231 : R1=-SC_2H_4OH, R2=-SC_2H_4OH
VK3-232 : R1=- $SCH_2CHOHCH_2OH$, R2=-$SCH_2CHOHCH_2OH$
VK3-233-2d : R1=-$SC_6H_{12}OH$, R2=-$SC_6H_{12}OH$
VK3-224 : R1=-NHC_2H_4 ($NC_2H_4OC_2H_4$), R2=-CH_3

Fig. 1. Structures of the synthesized VK3 analogues.

identified by matrix-assisted laser desorption/ionization-time of flight mass spectrometry as shown in Fig. S1. One milligram of Aβ1–40 peptide was dissolved in 1000 μl trifluoroethanol, and centrifuged (20,000× *g*) to sediment the insoluble particles. This Aβ1–40 solution was then dried under N_2 gas and resuspended in 1000 μl phosphate buffer, pH 7.4, to provide a stock solution, and stored at −80 °C until used.

2.5. Free radical assay

The level of free radicals (H_2O_2) induced by Aβ1–40 in cell free conditions was analyzed using the dichlorofluorescein diacetate (DCFH-DA) assay [35]. Dichlorofluorescein (DCF) diacetate was deacetylated with 50% (v/v) 0.05 M NaOH for 30 min and neutralized (pH 7.5) to a final concentration of 200 μM as a stock solution. This stock solution was kept on ice in the dark until further use. The reactions were carried out in a 96-well plate (200 μl/well) containing 25 μM of Aβ1–40 diluted from the peptide stock solution, 20 μM deacetylated DCF, 5 μM horseradish peroxidase, in Dulbecco's phosphate-buffered saline, pH 7.5. To determine the inhibitory effects of VK3 analogues on inhibition of free radical formation, VK3 analogues with concentrations of 1–1000 ng/ml were added and incubated at 37 °C. Fluorescence readings were recorded on a microplate reader (FlexStation 3, MD) with the excitation wavelength of 485 nm and the emission wavelength of 530 nm. The fluorescence intensity of DCF (H_2O_2 level) was measured every 6 h and from 0 to 72 h.

2.6. Peptide aggregation assay

Thioflavin-T (ThT) was used to monitor the aggregation state of Aβ1–40. Twenty-five μM of Aβ1–40 was freshly diluted from peptide stock solution in phosphate buffer, pH 7.4, for peptide aggregation assay. All samples containing a peptide concentration of 25 μM in the absence and presence of 100 ng/ml VK3 analogues and 3 μM ThT were incubated at 37 °C. Samples containing either Aβ peptide only (as a control) or Aβ with VK3 analogues, taken daily from day 0 to day 7, were used to measure the ThT intensity. The fluorescence measurement was performed on a microplate reader (FlexStation 3, MD) at 37 °C. The excitation and emission wavelengths were 440 nm and 485 nm, respectively.

2.7. Cell cultures

Human blastoma SH-SY5Y cells were cultured in minimum essential medium supplemented with 10% (v/v) heat-inactivated fetal bovine serum, 50% (v/v) F-12 nutrient mixture, and 1% (v/v) antibiotic mixture comprised of penicillin and streptomycin. Cells were kept at 37 °C in a humidified atmosphere of 5% CO_2. SH-SY5Y cells were plated at a density of 1×10^5 viable cells per well in 96-well plates for further analyses.

2.8. Cell viability assay

The cell viability was measured using the WST-1 assay [36]. Five hundred micromoles of Aβ1–40 peptide stock solution were initially prepared by dissolving 1 mg of Aβ1–40 in 1000 μl trifluoroethanol and centrifuging to sediment the insoluble particles. This peptide solution was dried under N_2 gas, redissolved in dimethyl sulfoxide, and incubated at 4 °C for 12 h to provide the final peptide stock solution [37]. For the viability assay, 1×10^5 cells were incubated in a 96-well microtiter plate containing either 25 μM incubated Aβ peptides only (as a positive control), diluted from the incubated peptide stock solution, or 25 μM incubated Aβ peptides, in the presence of VK3 analogues with concentrations ranging from 1 to 1000 ng/ml. The reaction was in a total volume of 200 μl per well for 24 h at 37 °C in a humidified atmosphere containing 5% CO_2 before cell viability was assayed. WST-1 solution (10 μl) was added to each well, and the wells were incubated for another 4−5 h at room temperature. The optical density was determined at 450 nm, using a microplate reader (FlexStation 3, MD).

2.9. Fourier-transform infrared (FT-IR) spectroscopy

To investigate the secondary structure of Aβ1–40 with or without VK3 analogues, a FT-IR spectrometer (Jasco, FT-IR/4100) equipped with an attenuated total reflection accessory was used to determine the conformation of Aβ1–40 during the aggregative process. One hundred microliters of 0.1 mM Aβ solution was coated on ZnSe crystals and dried overnight in a desiccator at room temperature. The spectra were recorded at 1500−1800 cm^{-1} with a 1 cm^{-1} interval. The peak was identified from the first derivation of the IR spectrum in the amide I region, and the secondary structure was analyzed using Original 6.0 software.

3. Results

3.1. Aβ1–40 aggregation in the presence and absence of VK3 analogues

Although VK3 is a well-known neurotoxic compound [38,39], its structure also contains several features found in some anti-amyloidogenic compounds [10,18–20] and in reactive oxygen species (ROS) scavenging compounds [40]. Therefore, 15 VK3 analogues, based on the fine structure of VK3 and shown in Fig. 1, were synthesized and used for numerical and experimental studies for their ability to inhibit the aggregation and neurotoxicity of Aβ1–40.

The key hallmark of AD pathogenesis is the formation of toxic Aβ1–40 plaques in the brain of AD patients [1,2]. Therefore, preventing or reducing the aggregation of Aβ has been the primary goal of a number of therapeutic strategies under development or in clinical trials [11–13]. In the present study, we examined the effects of VK3 analogues on the inhibition of Aβ aggregation using the Th-T fluorescence assay. Fig. 2(A) shows the ratio of Th-T fluorescence intensity of Aβ1–40 with VK3 analogues/Aβ1–40 alone at day 5. As shown in Fig. 2(A), several VK3 analogues, including VK3-2, VK3-6, VK3-8, VK3-9, VK3-10, VK3-199, VK3-221, and VK3-224, were found to inhibit the aggregation of Aβ1–40. Among these VK3 analogues, VK3-10, VK3-6, and VK3-9 were the most effective analogues for the inhibition of Aβ1–40 aggregation. In contrast, some VK3 analogues such as VK3-1, VK3-4, VK3-5, and VK3-233-2d, and especially VK3-4 and VK3-5 enhanced the aggregation of Aβ1–40.

3.2. Secondary structure of Aβ1–40 in the presence and absence of VK3 analogues

In the aggregation process, the conformation of Aβ1–40 is converted from either helix or random coil into β-sheet. Results from the aggregation assay showed that several VK3 analogues can inhibit the aggregation of Aβ1–40. Therefore, we examined these VK3 analogues to determine if they could also prevent the conformational change of Aβ1–40. Fig. 3(A−D) show the FT-IR spectra for Aβ1–40 in the presence of several VK3 analogues at day 1 and day 5. The conformation of Aβ1–40 in the presence of several VK3 analogues, including VK3-2, VK3-6, VK3-8, VK3-9, VK3-10, VK3-199, VK3-221, and VK3-224, remained largely in a random coil conformation at both day 1 and day 5, as the 1650 cm^{-1} major peak was an indication of random coil.

In contrast, the 1650 cm^{-1} peak that appeared in the FT-IR spectra of Aβ1–40 alone or in the presence of VK3-1, VK3-3, VK3-5, and VK3-232-2d at day 1 shifted to 1625 cm^{-1} at day 5. This indicated that Aβ1–40 converted to an extended β-sheet. These results were consistent with the Th-T aggregation assay, in which VK3-6, VK3-9, VK3-10, VK3-199, and VK3-221 inhibited the conformation change of Aβ1–40.

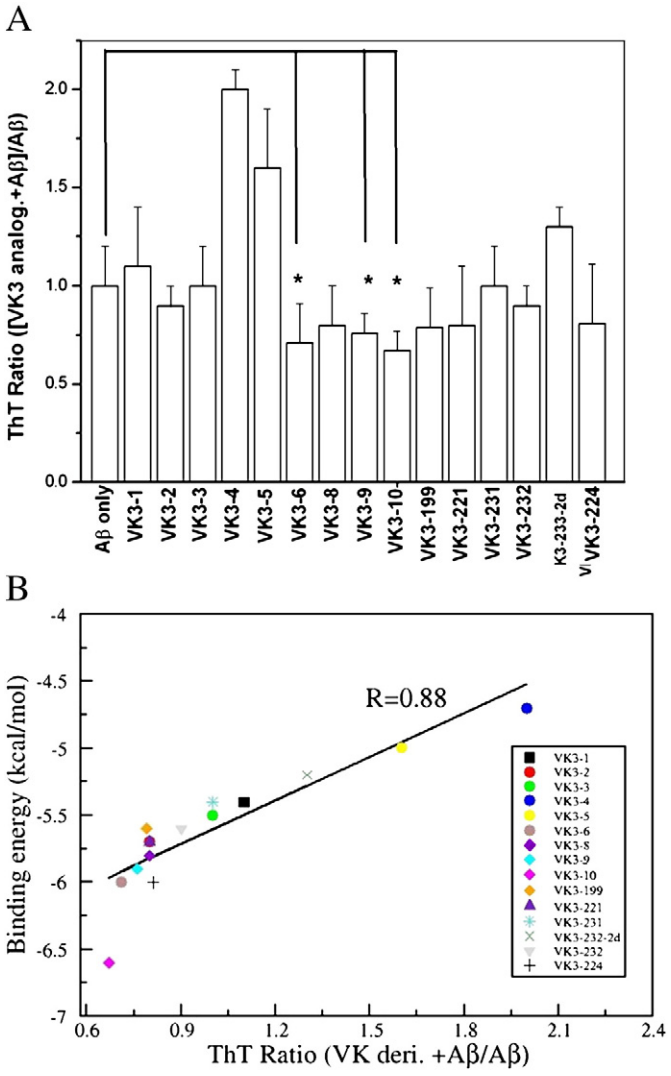

Fig. 2. Aggregation profile for Aβ1–40 in the presence and absence of VK3 analogues. (A) Aggregation of Aβ1–40 in the presence and absence of VK3 analogues determined by using the ratio of Th-T fluorescence intensity of (Aβ1–40 + VK3 analogues)/(Aβ1–40). The fluorescence intensity ratio presented here was obtained at day 5. VK3-2, VK3-6, VK3-8, VK3-9, VK3-10, VK3-199, VK3-221, VK3-232-2d, and VK3-224 are shown to effectively inhibit Aβ1–40 aggregation (*, $P<0.05$). (B) Plot of correlation between the binding energy and aggregation index (R = 0.88).

3.3. Cell viability in the presence and absence of VK3 analogues

Since previous results showed that several VK3 analogues can prevent Aβ aggregation and conformation change, their effects on the Aβ induced toxicity were then examined by cell viability assay. Fig. 4(A) shows the related cell viability in the presence of 100 ng/ml of VK3 analogue, incubated for 24 h. Unlike the results obtained in aggregation and secondary structural studies the results of Fig. 4(A) showed that only VK3-9 effectively reduced Aβ induced cell death at concentrations <100 ng/ml. Further analyses as depicted in Fig. S2 of SI showed that, with VK3-9 the cell viability was affected in a dose-dependent manner. Cell survival rate was increased to 50% with 1 ng/ml VK3-9, to 88% with 100 ng/ml VK3-9, and to 92% with 1000 ng/ml VK3-9.

For other VK3 analogues, including VK3-1, VK3-2, VK3-3, VK3-8, VK3-4, VK3-5, VK3-6, VK3-10, VK3-119, VK3-221, and VK3-231, the cell survival rate of SH-SY5Y cells was even much lower than in the presence of Aβ1–40 alone. The cell viability in the presence of these VK3 analogues were decreased with an increase of VK3 analogue concentration as depicted in Fig. S2 of SI. For VK3-232, VK3-233-2d, and VK3-224, the cell viability showed no difference compared to that of 25 μM Aβ1–40 alone (as a positive control).

3.4. VK3 analogues attenuated Aβ1–40 induced free radical formation

For some VK3 analogues such as VK3-10, the results obtained from cell viability assays were consistent with that obtained from aggregation assays. Because the production of ROS by Aβ peptide has been proposed as one of the possible mechanisms causing cell death [1,2,36], the role of VK3 analogues in free radical generation induced by Aβ1–40 was studied using the DCF assay. Fig. 5(A) shows the DCF fluorescence intensity of Aβ1–40 alone and in the presence of 100 ng/ml VK3 analogues, when incubated for 36 h. In Fig. 5(A), the DCF fluorescence intensity of Aβ1–40 in the presence of VK3-9 and VK3-5 was lower than the intensities with Aβ1–40 alone or with other VK3 analogues.

In comparison with the DCF intensity of Aβ1–40 alone, the DCF fluorescence intensity was decreased by 20% and 15% in the presence of 100 ng/ml VK3-9 and VK3-5, respectively, when incubated for 36 h. The intensity of DCF fluorescence was even further decreased as incubation time increased to 72 h. The DCF fluorescence intensity was further decreased by 25% and 40% for VK3-5 and VK3-9, at 72 h (Fig. S3 in SI), respectively, indicating that the free radical levels induced by Aβ peptides were effectively lowered by VK3-9 and VK3-5. The results obtained from free radical assays for VK3-9 are in agreement with the cell viability and aggregation assays, suggesting that the protection of SH-SY5Y cells against Aβ toxicity may be through the reduction of Aβ aggregation and subsequent induced free radical damage.

For the other VK3 analogues, the DCF fluorescence intensity of Aβ1–40 in the presence of VK3-1, VK3-2, VK3-3, VK3-8, VK3-10, VK3-199, VK3-231, and VK3-232-2d was even more pronounced than that of Aβ1–40 alone. This suggests that these VK3 analogues may be able to increase free radical levels. The DCF fluorescence intensity of Aβ1–40 in the presence of VK3-4 and VK3-6 was approximately equal to that of Aβ1–40 alone. This result could explain why VK3 analogues, such as VK3-10, prevent Aβ aggregation but fail to protect cells from Aβ induced cell toxicity due to the free radicals produced by these VK3 analogues.

3.5. Docking of VK3 analogues to Aβ1–40

Experimental studies showed that VK3-9 was the only VK3 analogue capable of protecting SH-SY5Y cells against Aβ induced toxicity. Other VK3 analogues, such as VK3-10 also inhibited Aβ aggregation more effectively than VK3-9. Therefore, we further analyzed the binding affinities of VK3 analogues to Aβ, to determine if additional VK3 analogues could be used as treatments for AD.

For numerical studies, to mimic the conformation of monomeric Aβ, we simulated the monomeric Aβ1–40 structure in an aqueous environment (see Fig. S4 in SI) and used this representative structure as a model for further docking studies of VK3 analogues to Aβ1–40. Fig. 6 shows the typical structure of Aβ1–40 when binding with various VK3 analogues. The related binding energies are summarized in Table 1.

In general, there are two main VK3 binding pockets in Aβ1–40. The first VK3 binding pocket is located at the central hydrophobic region around GLU 11-VAL 22, and the second binding pocket is located at the interface of the N- and C-terminus (Fig. 6). The VK3 analogues interacting at the first binding pocket include VK3-1, VK3-2, VK3-3, VK3-4 VK3-8, VK3-199, VK3-231, VK3-224, and VK3-232, whereas VK3-5, VK3-6, VK3-9, VK3-10, and VK3-221 may interact at the second binding pocket. The binding site of VK3-233-2d is close to the second binding site where it interacts with ASP 1-PHE 4 and ALA 30-VAL 40. Based on the calculated binding energies, the VK3 analogues located at the second binding pocket interact with Aβ with a higher affinity than the VK3 analogues located at the first binding site.

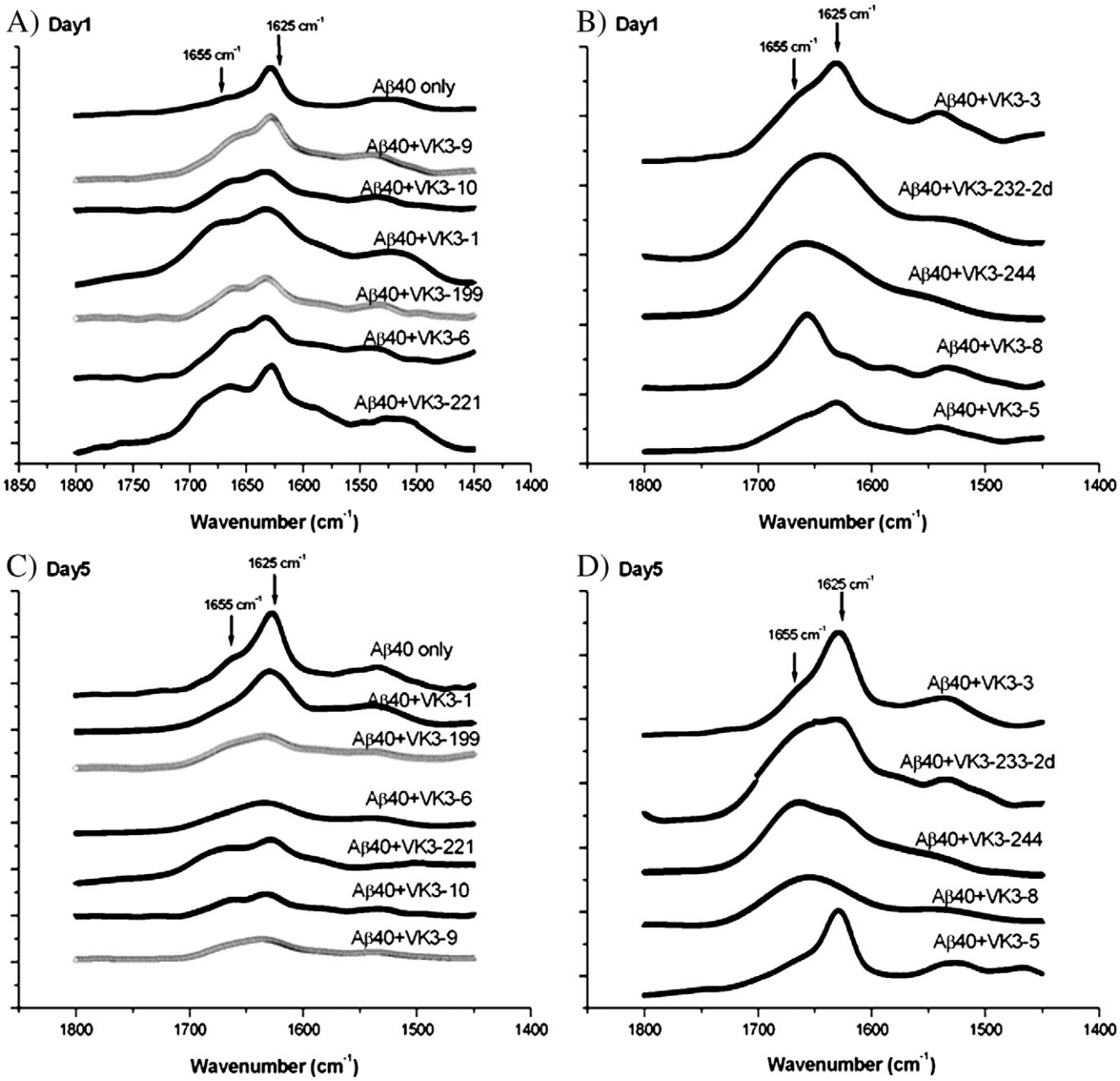

Fig. 3. FT-IR spectra of 25 μM Aβ1–40 in the presence of various VK3 analogues at day 1, (A) and (B), and day 5, (C) and (D). The concentration of VK3 analogues is 100 ng/ml. The peak at 1625 cm^{-1} represents the characteristic of β-sheet conformation.

Furthermore, the VK3 analogues located at the second binding pocket could be divided into two subgroups based on their binding energies. In general, the first subgroup bound to Aβ with a higher affinity than the second group. The first subgroup includes VK3-10, VK3-6, VK3-9, and VK3-221, whereas VK3-5 and VK3-233-2d belong to the second subgroup. Moreover, the binding energy of VK3-10 is the lowest among all VK3 analogues, indicating that this analogue is bound most tightly to Aβ. VK3-10 is surrounded by six residues TYR 10, GLU 11, VAL 12, PHE 20, VAL 36, and VAL 40 which are mainly located in the very central hydrophobic region.

Further analysis of hydrogen bonding patterns for the four typical VK3 analogues, VK3-4, VK3-5, VK3-221, and VK3-10, with different binding energies, is shown in Table I. As shown in Fig. 7(A) and (B), VK3-221 has the highest number of hydrogen bonds, but its binding affinity is lower than that of VK3-10. VK3-4, VK3-5, and VK3-10 have the same number of hydrogen bonds but their binding affinities are very different, suggesting that hydrogen bonds alone are not the key factor governing the binding affinity of the VK3 analogues to Aβ1–40. The fact that hydrogen bonding is not a key factor controlling binding affinity of VK3 analogues to Aβ peptides has been also observed in our previous study of β-sheet disrupting peptides [26].

To gain more insight into the binding affinity mechanisms of VK3 analogues to the aggregated form of Aβ, we performed docking studies of VK3 analogues to fibril forms of Aβ, using the structure previously reported [41], as shown in Fig. S8. As with the monomeric structure (Fig. 6), VK3 analogues have different binding positions in the best docking mode (Fig. S8(A)). The binding energies also displayed high correlation with the aggregation indices (Fig. S8(B)) with correlation

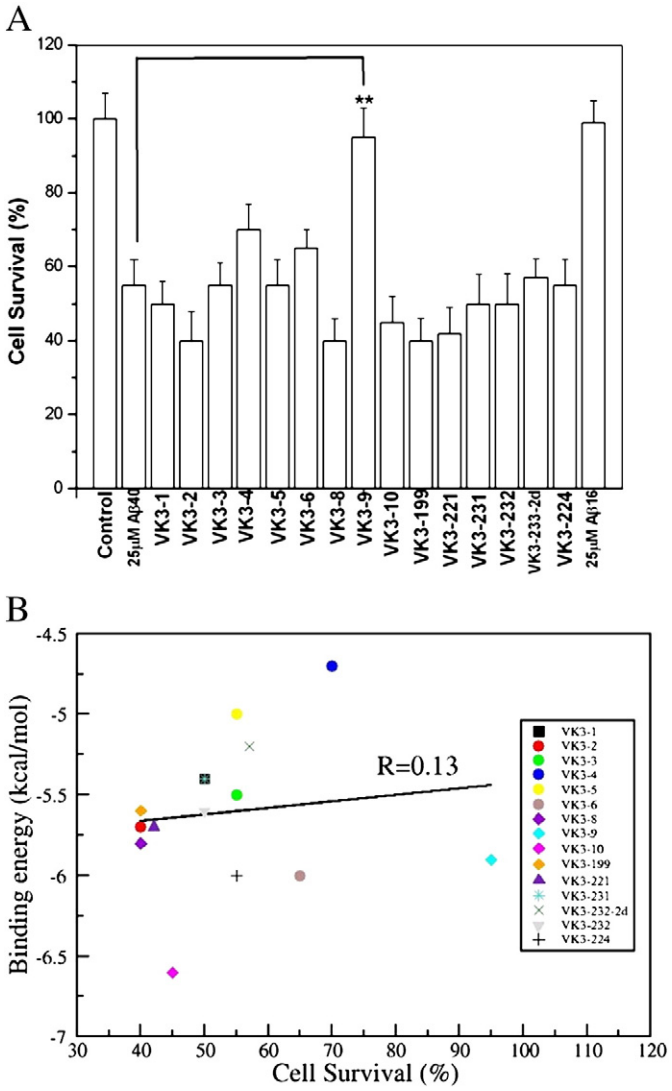

Fig. 4. Cell viability assay for the toxicity induced by Aβ1–40 in the presence and absence of Vk3 analogues. (A) Relative cell viability assessed by WST-1 assay in 25 μM of Aβ1–40 alone (as positive control) and in 25 μM of Aβ1–40 in the presence of 100 ng/ml of VK3 analogues incubated for 24 h. In the last column, Aβ1–16 which is not toxic to cells was used as a negative control. Results demonstrate that only VK3-9 effectively protect cells against Aβ-induced neurotoxicity (**, $P<0.01$). (B) The correlation between the binding energy and cell survival rate (R = 0.13).

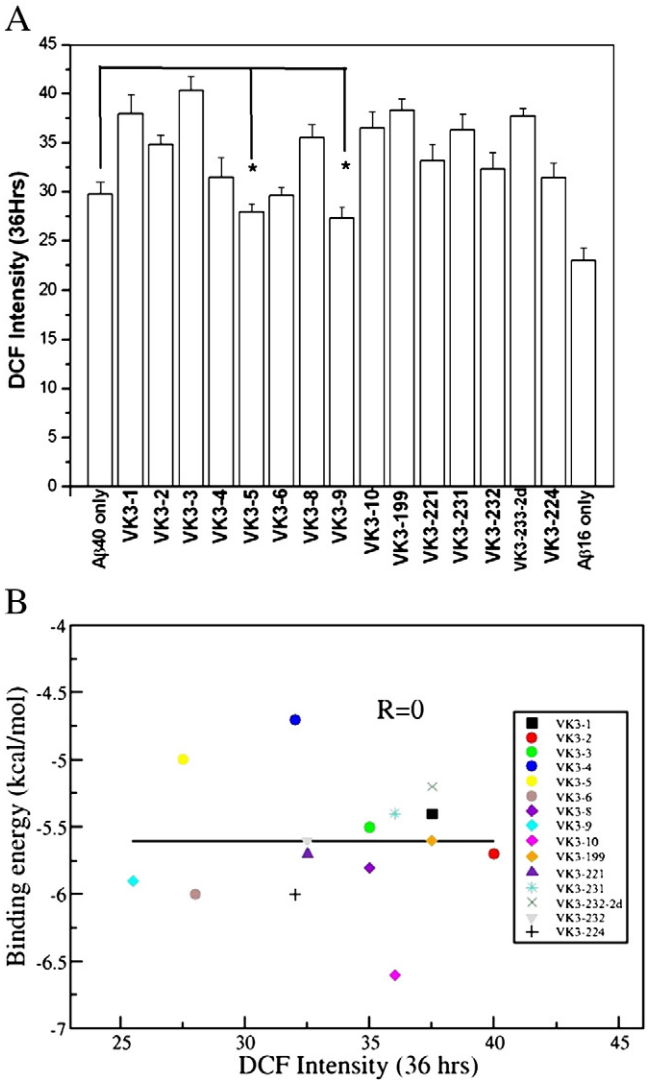

Fig. 5. Free radical assay for Aβ1–40 in the presence and absence of VK3 analogues. (A) Characterization of free radical generation for either 25 μM of Aβ1–40 alone or 25 μM of Aβ1–40 in the presence of 100 ng/ml of VK3 analogues, assessed by DCF-fluorescence assay. In the last column, Aβ1–16 which cannot produce free radicals was used as a negative control. Both VK3-9 and VK3-5 inhibit the free radicals induced by Aβ1–40 (* = $P<0.05$). (B) The correlation between the binding energy and DCF intensity (R = 0.0).

level $R = 0.75$. VK3-10 has the highest binding affinity, whereas VK3-9 is ranked fifth, suggesting that these compounds associate strongly with Aβ fibrils.

3.6. MM-PBSA simulation

To determine the binding properties, we computed the binding free energy ΔG_{bind} using the more accurate MM-PBSA method, which calculates several other energy terms (see SI for more details). Because MM-PBSA simulation is very time-consuming, we only choose representative compounds VK3-221, VK3-2, VK3-6, VK3-9, and VK3-10 based on previous docking results, and focused on the last two compounds because VK3-10 has the strongest binding affinity, whereas VK3-9, as shown by our results, is the most promising compound.

MD simulations of various times were performed for VK3-221, VK3-2, VK3-6, VK3-9, and VK3-10. As shown in Figs. S6 and S7, the equilibrium of complexes were reached at different times when the interaction energies between VK3 analogues and Aβ1–40 became saturated. As an example, for VK3-9, in trajectory 6 the system reached equilibrium within 22 ns, and the equilibration time was approximately 260 ns for the second trajectory (Fig. S6). A similar situation was also observed for VK3-10 (Fig. S7) and for other VK3 analogues (data not shown).

Snapshots collected in an equilibrium state were used to estimate ΔG_{bind} by the MM-PBSA method (see SI for more details). The final results are shown in Table 2. In agreement with docking and experimental results, VK3-9 and VK3-10 have the lowest ΔG_{bind}, indicating that they have higher binding affinities than VK3-221, VK3-2, and VK3-6. With the exception of VK3-221, the entropic contributions are almost the same for the other VK3 analogues (Table 2). For VK3-6 and VK3-10, the contributions of vdW interactions dominated over that of electrostatic forces, and for VK3-9, VK3-221, and VK3-2, the VdW and electrostatic interactions had almost the same contributions. The nonpolar energies, ΔG_{sur}, were not sensitive but this does not apply to the polar energies, ΔG_{PB}.

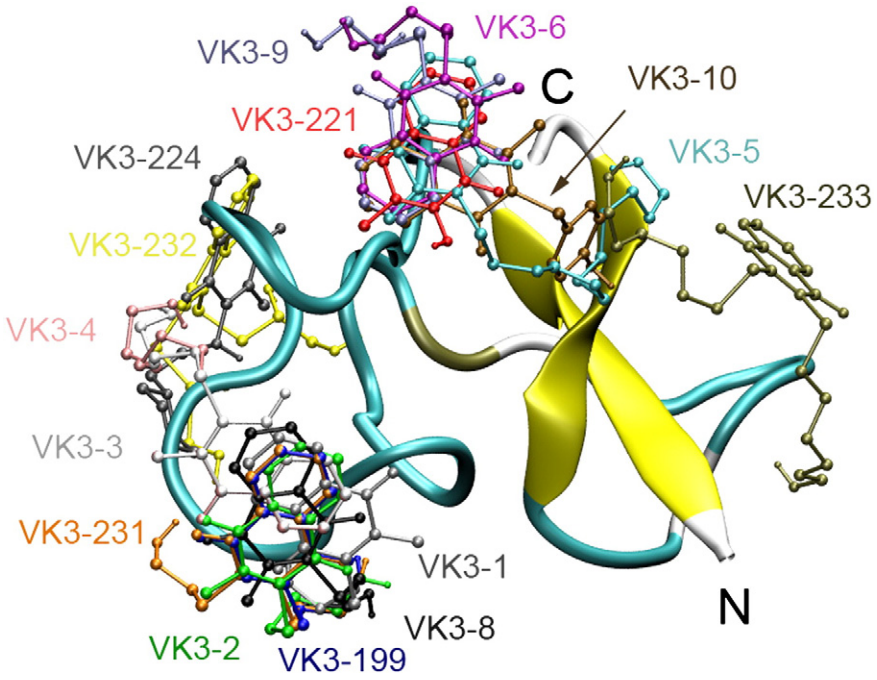

Fig. 6. The best docking mode of VK3 analogue binding sites obtained using Model-5 of Aβ1–40. The binding site residues which are close to VK3 analogues are listed as follows: **VK3-1**: GLU11, LEU17, VAL18, PHE19, and PHE20;. **VK3-2**: GLU11, LEU17, VAL18, PHE19, PHE20, and ALA21;. **VK3-3**: GLU11, VAL12, HIS13, HIS14, GLN15, LYS16, PHE19, and PHE20;. **VK3-4**: TYR10, GLU11, VAL12, HIS13, HIS14, GLN15, LYS16, PHE19, and PHE20;. **VK3-5**: TYR10, GLU11, VAL12, HIS13, GLN15, PHE20, VAL36, VAL39, and VAL40;. **VK3-6**: SER8, TYR10, GLU11, VAL12, and HIS13;. **VK3-8**: GLU11, LEU17, VAL18, PHE19, PHE20, and ALA21;. **VK3-9**: SER8, TYR10, GLU11, VAL12, HIS13, and VAL40;. **VK3-10**: TYR10, GLU11, VAL12, PHE20, VAL36, and VAL40;. **VK3-199**: GLU11, LEU17, VAL18, PHE19, and PHE20;. **VK3-221**: TYR10, GLU11,VAL12, HIS13, and PHE20;. **VK3-224**: ASP7, HIS14, LYS16, LEU17, GLU22, ASP23, VAL24, and SER26;. **VK3-231**: GLU11, LYS16, LEU17, VAL18, PHE19, PHE20, and ALA21;. **VK3-232**: ASP7, HIS14, LYS16, LEU17, VAL18, GLU22, ASP23, VAL24, and SER26;. **VK3-233-2d**: ASP1(N), ALA2, PHE4, TYR10, PHE20, ALA30, ILE31, ILE32, VAL36, GLY38, and VAL40.

3.7. Correlation of binding energy and experimental properties

The correlation between binding energies and the experimental properties, such as aggregation index, free radical levels, and cell viability are shown in Figs. 2(B), 4(B) and 5(B). As shown, only the aggregation indices and binding energies show a good correlation, and there was no correlation between binding energies and free radical levels or cell viability. The correlation index, R value, of aggregation and binding energy was >0.8, indicating that VK3 analogues bind to Aβ and inhibit aggregation.

4. Discussion

ROS are major toxic species which damage neurons, induce cell death, and which are highly correlated with Aβ aggregation [1,2,36]. The development of anti- amyloidogenic and antioxidant agents has been the main target for the therapeutic treatment of Alzheimer's disease. Numerous studies have focused on identifying effective compounds which inhibit the aggregation of monomeric Aβ or prevent formation of the ROS generated by Aβ [11,13].

The deficiency of vitamin K has been demonstrated to be related to pathogenesis of AD [27,42]. Supplementation of vitamin K may prevent AD [27,42]. Therefore, based on previous studies [27,42], we synthesized 15 VK3 analogues and determined their effects on Aβ induced neurotoxicity using numerical and experimental approaches. Our results show that several VK3 analogues such as VK3-10, VK3-9, and VK3-6 can strongly bind to Aβ1–40 and inhibit the aggregation of Aβ *in vitro*, but only VK3-9 has a protective effect by reducing Aβ induced toxicity. MD simulation studies show that VK3-10, VK3-9, and VK3-6 strongly interact with Aβ and possibly inhibit its aggregation.

The reason that most VK3 analogues failed to protect SH-Y5Y cells against Aβ induced neurotoxicity may be because most VK3 analogues can also produce free radicals and cause the death of these cells. It is interesting to note that VK3-4 and VK3-5 promoted the aggregation of Aβ1–40. A possible reason for the effects of VK3-4 and VK3-5 on Aβ aggregation may be similar to that of Congo Red at low concentrations, which can enhance the aggregation of Aβ into fibrils [43]. However, a detailed mechanism will require further investigation.

For VK3-9, 100 ng/ml was sufficient to protect SH-Y5Y cells against Aβ induced toxicity, and cell survival rate was 90%. Furthermore, VK3-9 alone was not toxic and was capable of inhibiting the free radical generation and aggregation of Aβ. The effective dose of VK3-9 for a 90% cell survival rate was approximately 100 ng/ml (~0.36 μM), which was comparable to the IC_{50} of curcumin (0.19–0.98 μM) [14,15,20,21].

The simulation of VK3 analogue docking to Aβ monomer suggests that there are two main VK3 binding sites. One is located at the central hydrophobic region, and the other is located at the N- and C-terminal interfaces (Fig. 6). The strongest VK3 analogues, such as VK3-10 and VK3-9, interact with Aβ at both the central and C-terminal hydrophobic regions, indicating that the hydrophobic region may play a key role in the aggregation and toxicity of Aβ. In the case of mature fibrils, binding sites are more scattered when compared to the monomeric state (Fig. S8). However, VK3-9 and VK3-10 are located at the same position and this is also valid for the monomeric state (Fig. 6). It would be very interesting to verify our prediction on location of binding sites of VK3 analogues by experimental results. It is also important to stress that the simulation provides insights on the binding mechanism, suggesting that the binding of VK3 analogues to Aβ are mainly governed by van der Waals and electrostatic interactions and not by hydrogen bonding interactions. Knowledge of the contributions of each interaction strategy to binding affinity is very useful for designing new potential lead drugs for successful AD treatment. In this regard, MD simulation is a good complement to experiment tools for drug design.

The structural features of VK3 analogues are similar in configuration to other anti-amyloidogenic compounds such as curcumin and myricetin, which contain aromatic moieties [44]. Furthermore, the interaction modes of VK3 analogues with Aβ are very similar to that of curcumin binding to Aβ [43]. Recently, a study of the interaction of Aβ1–42 and

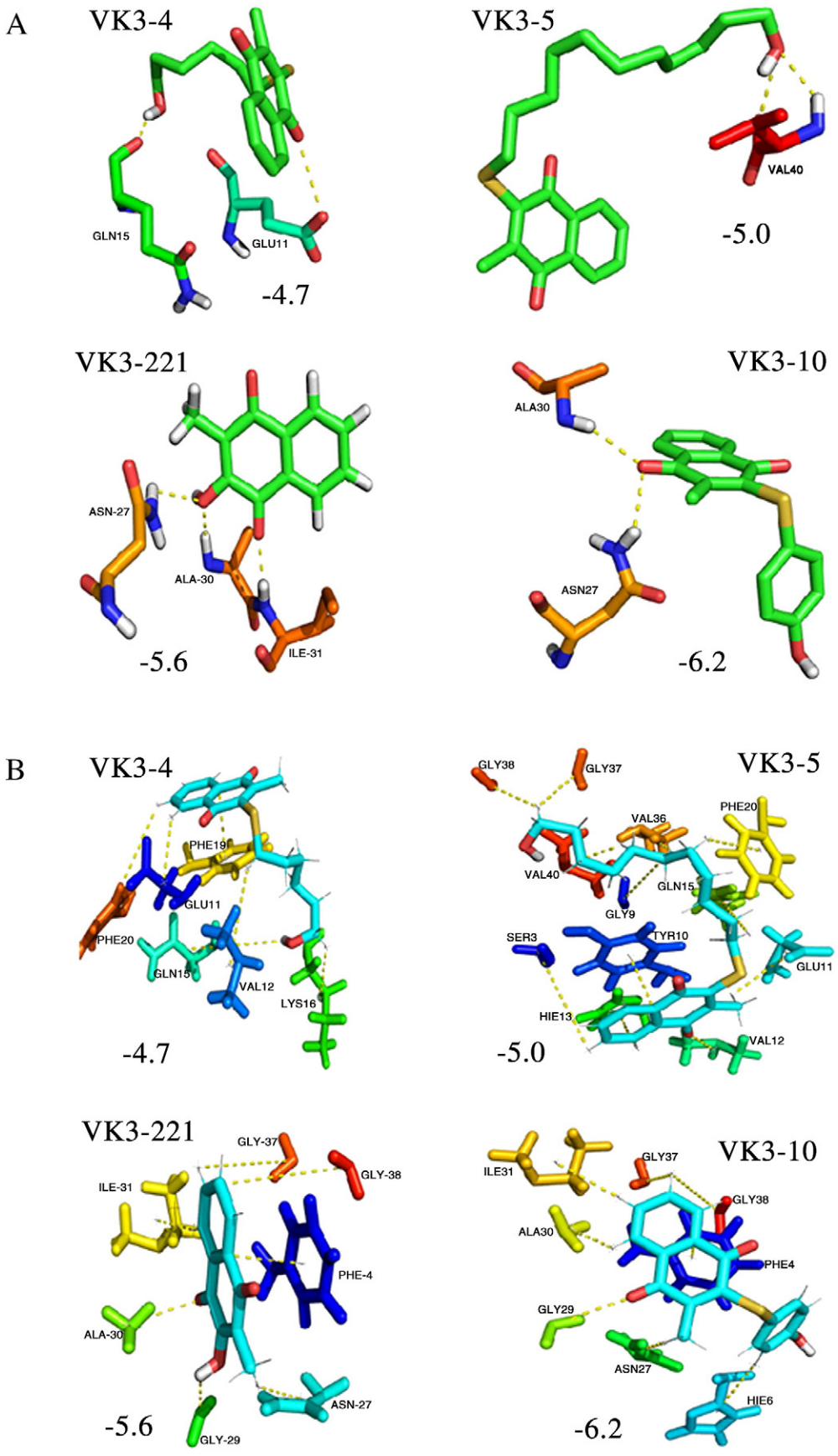

Fig. 7. Typical hydrogen bond networks (A) and side chain contacts (B) for backbone of VK3-4, VK3-5, VK3-221, and VK3-10. There are 6, 12, 7, and 8 side chain contacts for VK3-4, VK3-5, VK3-221, and VK3-10, respectively. Binding energies (in kcal/mol) are shown next to the depictions.

Table 1
Binding free energies (in kcal/mol) of 15 VK3 analogues to Aβ1–40 peptide obtained by the docking method. Experimental results on cell survival rate, free radical generation, and aggregation percentages are also shown.

VK3 analogues	ΔG_{bind} (kcal/mol)	Cell survival rate (%)	Free radical generation	Aggregation percentage
VK3-1	−5.4	50	37.5	1.1
VK3-2	−5.7	40	40	0.8
VK3-3	−5.5	55	35	1
VK3-4	−4.7	70	32	2
VK3-5	−5.0	55	27.5	1.6
VK3-6	−6.0	65	28	0.71
VK3-8	−5.8	40	35	0.8
VK3-9	−5.9	95	25.5	0.76
VK3-10	−6.6	45	36	0.67
VK3-119	−5.6	40	37.5	0.79
VK3-221	−5.7	42	32.5	0.8
VK3-231	−5.4	50	36	1
VK3-232	−5.6	50	32.5	0.9
VK3-233-2d	−5.2	57	37.5	1.3
VK3-224	−6	55	32	0.81

VK3, vitamin K3; Aβ, amyloid-beta.

curcumin by solid state nuclear magnetic resonance indicated that curcumin may interact with residues 12 and 17–21 of Aβ1–42 through an aromatic group [44]. The simulation models of VK3-10 and Aβ1–40 complexes as shown in Fig. 6(B) also suggest a similar interaction mode as curcumin and Aβ1–42, in which VK3-9 and VK3-10 may interact with residues of SER 8-PHE 20 of Aβ1–40 and the aromatic carbons adjacent to the methoxy and/or hydroxy group known to form hydrogen bonds with residues of Aβ1–40.

Further MM-PBSA simulation also indicates that the binding affinities of these VK3 analogues are also comparable to curcumin. The binding free energies for VK3-9 and VK3-10 are $\Delta G_{bind} = -15.41 \pm 3.44$ and -12.42 ± 3.87 kcal/mol (Table 2), respectively. Within error bars, ΔG_{bind} of VK3-9 and VK3-10 are the same as that obtained by MM-PBSA for curcumin, with $\Delta G_{bind} = -14.3$ kcal/mol [45]. This value is very close to the experimental estimate $\Delta G_{bind} = -13.3$ kcal/mol [46]. Taken together, our numerical and experimental results show that VK3-9 and VK3-10 are as potent as curcumin in preventing aggregation of Aβ, with inhibition constants of approximately a 0.1 μM range [14].

In conclusion, our present study shows that VK3-9 can effectively inhibit the aggregation of Aβ, reduce the free radicals produced by Aβ, and protect cells against Aβ induced toxicity. Although most VK3 analogues do not have protective effects for cells against Aβ induced toxicity, our simulation study indicates that some of the VK3 analogues, such as VK3-10, have a high potential for further development as anti-amyloidogenic drugs for AD treatment.

Supplementary data to this article can be found online at http://dx.doi.org/10.1016/j.bbagen.2012.12.026.

Acknowledgement

The work was supported by Narodowe Centrum Nauki in Poland (grant No 2011/01/B/NZ1/01622 to M. S. L) and Department of Science and Technology at Ho Chi Minh City, Vietnam and by grants from National Science Council of Taiwan, ROC (NSC99-2627-M-715-001 and NSC100-2627-M-715-001 to Y. C. C.). Allocation of CPU time at Supercomputer TASK (Gdansk, Poland) is highly appreciated.

References

[1] D.A. Butterfield, T. Reed, S.F. Newman, R. Sultana, Roles of amyloid beta-peptide-associated oxidative stress and brain protein modifications in the pathogenesis of Alzheimer's disease and mild cognitive impairment, Free Radic. Biol. Med. 43 (2007) 658–677.
[2] S.M. Yatin, S. Varadarajan, C.D. Link, D.A. Butterfield, In vitro and in vivo oxidative stress associated with Alzheimer's amyloid beta-peptide (1–42), Neurobiol. Aging 20 (1999) 325–330.
[3] D.J. Selkoe, The molecular pathology of Alzheimer's disease, Neuron 6 (1991) 487–498.
[4] I. Dolev, D.M. Michaelson, The nucleation growth and reversibility of amyloid-beta deposition in vivo, J. Alzheimers Dis. 10 (2006) 291–301.
[5] J. McLaurin, D. Yang, C.M. Yip, P.E. Fraser, Modulating factors in amyloid-beta fibril formation, J. Struct. Biol. 130 (2000) 259–270.
[6] D.M. Skovronsky, R.W. Doms, V.M. Lee, Detection of a novel intraneuronal pool of insoluble amyloid beta protein that accumulates with time in culture, J. Cell Biol. 141 (1998) 1031–1039.
[7] M.P. Lambert, A.K. Barlow, B.A. Chromy, C. Edwards, R. Freed, M. Liosatos, T.E. Morgan, I. Rozovsky, B. Trommer, K.L. Viola, P. Wals, C. Zhang, C.E. Finch, G.A. Krafft, W.L. Klein, Diffusible nonfibrillar ligands derived from Abeta1–42 are potent central nervous system neurotoxins, Proc. Natl. Acad. Sci. U.S.A. 95 (1998) 6448–6453.
[8] A.E. Roher, M.O. Chaney, Y.M. Kuo, S.D. Webster, W.B. Stine, L.J. Haverkamp, A.S. Woods, R.J. Cotter, J.M. Tuohy, G.A. Krafft, B.S. Bonnell, M.R. Emmerling, Morphology and toxicity of Abeta-(1–42) dimer derived from neuritic and vascular amyloid deposits of Alzheimer's disease, J. Biol. Chem. 271 (1996) 20631–20635.
[9] D.M. Hartley, D.M. Walsh, C.P. Ye, T. Diehl, S. Vasquez, P.M. Vassilev, D.B. Teplow, D.J. Selkoe, Protofibrillar intermediates of amyloid beta-protein induce acute electrophysiological changes and progressive neurotoxicity in cortical neurons, J. Neurosci. 19 (1999) 8876–8884.
[10] F. Re, C. Airoldi, C. Zona, M. Masserini, B. La Ferla, N. Quattrocchi, F. Nicotra, Beta amyloid aggregation inhibitors: small molecules as candiate drugs from therapy of Alzheimers' disease, Curr. Med. Chem. 17 (2010) 2990–3006.
[11] V.M. Lee, Amyloid binding ligands as Alzheimer's disease therapies, Neurobiol. Aging 23 (2002) 1039–1042.
[12] Q. Nie, X.G. Du, M.Y. Geng, Small molecule inhibitors of amyloid β peptide aggregation as a potential therapeutic strategy for Alzheimer's disease, Acta Pharmacol. Sin. 32 (2011) 545–551.
[13] S.E. Kolstoe, S.P. Wood, Drug targets for amyloidosis, Biochem. Soc. Trans. 38 (2010) 466–470.
[14] K. Ono, K. Hasegawa, H. Naiki, M. Yamada, Curcumin has potent anti-amyloidogenic effects for Alzheimer's beta-amyloid fibrils in vitro, J. Neurosci. Res. 75 (2004) 742–750.
[15] Y. Porat, A. Abramowitz, E. Gazit, Inhibition of amyloid fibril formation by polyphenols: structural similarity and aromatic interactions as a common inhibition mechanism, Chem. Biol. Drug Des. 67 (2006) 27–37.
[16] H.A. Lashuel, D.M. Hartley, D. Balakhaneh, A.A. Ggarwal, S. Teichberg, D.J.E. Callaway, New class of inhibitors of amyloid-β fibril formation, J. Biol. Chem. 277 (2002) 42881–42890.
[17] G.P. Lim, T. Chu, T. Morihara, F. Yang, B. Teter, O. Ubeda Jr., N. Salem, S.A. Frautschy, G.M. Cole, A diet enriched with the omega-3 fatty acid docosahexaenoic acid reduces amyloid burden in an aged Alzheimer mouse model, J. Neurosci. 25 (2005) 3032–3040.
[18] K. Ono, Y. Yoshiike, A. Takashima, K. Hasegawa, H. Naiki, M. Yamada Vitamin, A exhibits potent antiamyloidogenic and fibril-destabilizing effects *in vitro*, Exp. Neurol. 189 (2004) 380–392.
[19] M. Hirohata, K. Ono, H. Naiki, M. Yamada, Non-steroidal antiinflammatory drugs have anti-amyloidogenic effects for Alzheimer's β-amyloid fibrils *in vitro*, Neuropharmacology 49 (2005) 1088–1099.
[20] K. Ono, K. Hasegawa, H. Naiki, M. Yamada, Anti-Parkinsonian agents have anti-amyloidogenic activity for Alzheimer's β-amyloid fibrils *in vitro*, Neurochem. Int. 48 (2006) 275–285.
[21] F. Yang, G.P. Lim, A.N. Begum, O.J. Ubeda, M.R. Simmons, S.S. Ambegaokar, P. Chen, R. Kayed, C.G. Glabe, S.A. Frautschy, G.M. Cole, Curcumin inhibits formation

Table 2
Binding free energies (in kcal/mol) of VK3 analogues to Aβ1–40 peptide obtained by the MM-PBSA method.

VK3 analogues	ΔE_{elec}	ΔE_{vdw}	ΔG_{sur}	ΔG_{PB}	$-T\Delta S$	ΔG_{bind}
VK3-221	−13.77 ± 1.02	−17.05 ± 2.59	−2.09 ± 0.23	20.91 ± 1.87	5.88 ± 0.12	−6.12 ± 3.25
VK3-2	−19.59 ± 8.75	−21.76 ± 5.37	−2.73 ± 0.51	24.41 ± 6.27	10.27 ± 0.47	−9.41 ± 6.30
VK3-6	41.66 ± 22.0	−19.99 ± 5.18	−2.49 ± 0.55	−32.15 ± 24.30	9.60 ± 1.80	−3.37 ± 3.72
VK3-9	−29.06 ± 9.67	−27.75 ± 3.29	−3.35 ± 0.24	31.94 ± 7.85	12.81 ± 0.52	−15.41 ± 3.44
VK3-10	−6.83 ± 2.12	−29.31 ± 6.32	-3.21 ± 0.40	14.91 ± 3.99	12.03 ± 0.48	−12.42 ± 3.87

MM-PBSA, molecular mechanics-Poisson Boltzmann surface area; VK3, vitamin K3; Aβ, amyloid-beta.

of amyloid-β oligomers and fibrils, binds plaques, and reduces amyloid *in vivo*, J. Biol. Chem. 280 (2005) 5892–5901.
[22] K. Ono, K. Hasegawa, H. Naiki, M. Yamada, Antiamyloidogenic activity of tannic acid and its activity to destabilize Alzheimer's β-amyloid fibrils *in vitro*, Biochim. Biophys. Acta 1690 (2004) 193–202.
[23] K. Ono, K. Hasegawa, H. Naiki, M. Yamada, Preformed β-amyloid fibrils are destabilized by coenzyme Q10 *in vitro*, Biochem. Biophys. Res. Commun. 330 (2005) 111–116.
[24] K. Ono, M. Hirohata, M. Yamada, Lipoic acid exhibits antiamyloidogenicity for β-amyloid fibrils *in vitro*, Biochem. Biophys. Res. Commun. 341 (2006) 1046–1052.
[25] K. Ono, M. Hirohata, M. Yamada, Ferulic acid destabilizes preformed β-amyloid fibril *in vitro*, Biochem. Biophys. Res. Commun. 336 (2005) 444–449.
[26] M.H. Viet, S.T. Ngo, N.S. Lam, M.S. Li, Inhibition of aggregation of amyloid peptides by beta-sheet breaker peptides and their binding affinity, J. Phys. Chem. B 115 (2011) 7433–7446.
[27] A.C. Allison, The possible role of vitamin K deficiency in the pathogenesis of Alzheimer's disease and in augmenting brain damage associated with cardiovascular disease, Med. Hypotheses 57 (2001) 151–155.
[28] M. Coles, W. Bicknell, A.A. Watson, D.P. Fairlie, D.J. Craik, Solution structure of amyloid beta-peptide(1-40) in a water-micelle environment. Is the membrane-spanning domain where we think it is? Biochemistry 37 (1998) 11064–11077.
[29] W. van Gunsteren, S.R. Billeter, A.A. Eising, P.H. Hünenberger, P. Krüger, A.E. Mark, W. Scott, I. Tironi, Biomolecular Simulation: The GROMOS96 Manual and User Guide, Vdf Hochschulverlag AG an der ETH, Zurich, 1996.
[30] M.F. Sanner, Python a programming language for software integration and development, J. Mol. Graph. Model. 17 (1999) 57–61.
[31] O. Trott, A.J. Olson, AutoDock Vina: improving the speed and accuracy of docking with a new scoring function, efficient optimization, and multithreading, J. Comput. Chem. 31 (2010) 455–461.
[32] G.M. Morris, D.S. Goodsell, R. Huey, A.J. Olson, Distributed automated docking of flexible ligands to proteins: parallel applications of AutoDock 2.4, J. Comput. Aided Mol. Des. 10 (1998) 293–304.
[33] D.F. Shanno, Math. Comput. 24 (1970) 647–656.
[34] C.P. Chen, Y.Z. Liu, K.S. Shia, H.Y. Tseng, Synthesis and anticancer evaluation of Vitamin K3 analogues, Bioorg. Med. Chem. Lett. 12 (2002) 2729–2732.
[35] R. Cristina, C.F. Yang, P.M. Ronald, Phenoxyl free radical formation during the oxidation of the fluorescent dye 2′, 7′-dichloro-fluorescein by horseradish peroxidase, J. Biol. Chem. 274 (1999) 28161–28168.
[36] M.Q. Liao, Y.J. Lea, Y.X. Chang, H.B. Huang, T.H. Lin, C.L. Chyan, Y.C. Chen, The correlation between neurotoxicity, aggregative ability and secondary structure studied by sequence truncated Aβ peptides, FEBS Lett. 581 (2007) 1161–1165.
[37] H. LeVine III, Alzheimer's β-peptide oligomer formation at physiologic concentrations, Anal. Biochem. 335 (2004) 81–90.
[38] G. Loor, J. Kondapalli, J.M. Schriewer, N.S. Chandel, Hoek T.L. Vanden, P.T. Schumacker, Menadione triggers cell death through ROS-dependent mechanisms involving PARP activation without requiring apoptosis, Free Radic. Biol. Med. 49 (2010) 1925–1936.
[39] R. Sasaki, Y. Suzuki, Y. Yonezawa, Y. Ota, Y. Okamoto, Y. Demizu, P. Huang, H. Yoshida, K. Sugimura, Y. Mizushina, DNA polymerase gamma inhibition by vitamin K3 induces mitochondria-mediated cytotoxicity in human cancer cells, Cancer Sci. 99 (2008) 1040–1048.
[40] D.W. Lamson, S.M. Plaza, The anticancer effects of vitamin K, Med. Rev. 8 (2003) 303–318.
[41] A.T. Petkova, R.D. Leapman, Z. Guo, W.M. Yau, M.P. Mattson, R. Tycko, Self-propagating molecular-level polymorphism in Alzheimer's beta-amyloid fibrils, Science 307 (2005) 262–265.
[42] N. Presse, B. Shatenstein, M.J. Kergoat, G. Ferland, Low vitamin K intakes in community-dwelling elders at an early stage of Alzheimer's disease, J. Am. Diet. Assoc. 108 (2008) 2095–2099.
[43] Y.S. Kim, T.W. Randolph, M.C. Manning, F.J. Stevens, J.F. Carpenter, Congo red populates partially unfolded states of an amyloidogenic protein to enhance aggregation and amyloid fibril formation, J. Biol. Chem. 278 (2003) 10842–10850.
[44] S.T. Ngo, M.S. Li, Curcumin binds to Aβ40 peptides and fibrils stronger than Ibuprofen and Naproxen, J. Phys. Chem. B 116 (2012) 10165–10175.
[45] E.K. Ryu, Y.S. Choe, K.H. Lee, Y. Choi, B.T. Kim, Curcumin and dehydrozingerone derivatives: synthesis, radiolabeling, and evaluation for β-amyloid plaque imaging, J. Med. Chem. 49 (2006) 6111–6119.
[46] Y. Masuda, M. Fukuchi, T. Yatagawa, M. Tada, K. Takeda, K. Irie, K. Akagi, Y. Monobe, T. Imazawa, K. Takegoshi, Solid-state NMR analysis of interaction sites of curcumin and 42-residue amyloid β-protein fibrils, Bioorg. Med. Chem. 19 (2011) 5967–5974.